# MULTIGROUP RADIATION HYDRODYNAMICS MODELING OF SUPERNOVA 1987A

S.Blinnikov[1,2], O.Bartunov[2], P.Lundqvist[3], V.Utrobin[1], K.Nomoto[4] R.Eastman[5], S.E.Woosley[5,6]

Received ________________; accepted ________________

[1]Institute for Theoretical and Experimental Physics, 117259, Moscow, Russia

[2]Sternberg Astronomical Institute, Moscow, Russia

[3]Stockholm Observatory, S-133 36 Saltsjöbaden, Sweden

[4]Tokyo University

[5]General Studies Group; Lawrence Livermore National Laboratory; Livermore CA 94550

[6]UCO/Lick Observatory, University of California, Santa Cruz, CA 95064



## ABSTRACT

The light curve of Supernova 1987A is calculated using the hydrocode `STELLA`, with a multi-group approach to radiation transport. Two progenitor models have been studied in some detail, the evolutionary model of Nomoto & Hashimoto (1988), Saio, Nomoto & Kato (1988) and non-evolutionary model of Utrobin (1990).

*Subject headings:* stars: supernovae – radiative transfer – hydrodynamics

## 1. The Code STELLA

From its inception, the code STELLA has incorporated implicitly differenced hydrodynamics and radiative transfer. The method uses the time-dependent equations for the angular moments of intensity averaged over fixed frequency bands. The number of those frequency groups at current workstation computing power (up to 100) allows one to have a reasonably accurate representation of non-equilibrium radiation. STELLA applies the equilibrium diffusion only at very large optical depth (typically, larger than 300).

The Eddington factors for each energy group are found by a method which uses the ideas of the Feautrier technique, but instead of following the block-elimination scheme of Feautrier STELLA uses the elimination technique due to Zlatev which works for matrices of arbitrary sparsity patterns.

In the equation of state we take into account ionization and recombination. The extinction is consistent with the equation of state.

All space and frequency derivatives are replaced by finite differences. For the discretization STELLA uses up to 300 zones for the Lagrangean coordinate and up to 100 frequency bins (i.e. energy groups). We thus get a system of ordinary differential equations (ODE) for the evolution



of radius, velocity and temperature in each Lagrangean zone and for Eddington radiation energy and flux in each frequency group in each Lagrangean zone. This is a version of the method of lines which here results in tens thousands of ODE. This huge system of ODE is solved by an implicit high-order (in time) predictor-corrector method based on the methods due to Gear and Brayton et al. The use of a scheme which is implicit not only in the radiative transfer but also in the hydrodynamics allows one to overcome the Courant restriction on the time-step and to apply the hydro-code not only to dynamic problems but also to situations where hydrostatic equilibrium prevails.

The Eddington factors $f_{\rm E}$ are computed separately for each energy group in each mass zone. To solve large systems of sparse linear equations appearing in the corrector iterations of the scheme STELLA again uses the technique due to Zlatev which gives one a very flexible scheme in comparison with more usual block elimination.

STELLA computes the gamma-ray transfer (in one-group approximation) for the non-local deposition of the energy of radio-active nuclei.

As in earlier versions, STELLA calculates variable Eddington factors not on every time step but, following the ideas of the method of quasi-diffusion (Goldin) after a prescribed number of steps, $N_{\rm Edd}$ ($N_{\rm Edd} = 50$ in the current implementation). The variable Eddington factors are computed in STELLA with full account of scattering and redshifts in each energy group.

Most important advance of the STELLA is the use of tables of realistic opacities with expansion effect in lines taken into account according to Eastman & Pinto.

## 2. Progenitor Models and Hydro Runs

The evolutionary model of Nomoto & Hashimoto (1988), Saio, Nomoto & Kato (1988) was studied in the runs nommxf, nommxfab, nommxfhi, nommixf for the mixed composition in Fig. 3 and in the run unmx for unmixed composition in Fig. 2 - see Table 1. The density structure of the presupernova model was the same for both compositions, see Fig. 1.



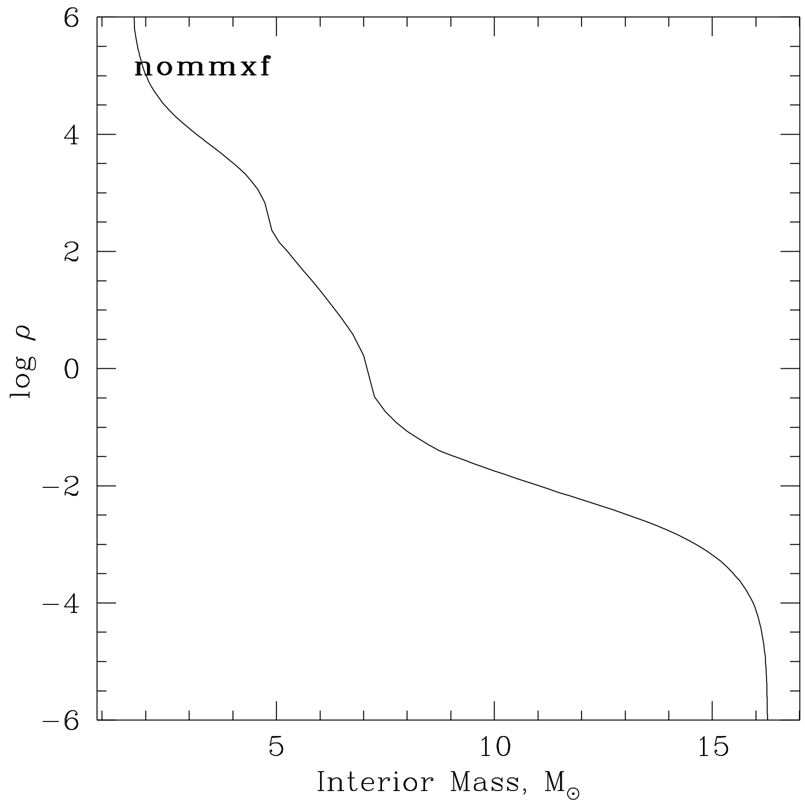


Fig. 1.— Density as a function of interior mass, $M_r$, in all models from Nomoto et al. (1988), with presupernova mass 16.27 $M_\odot$mass cut is 1.6 $M_\odot$.

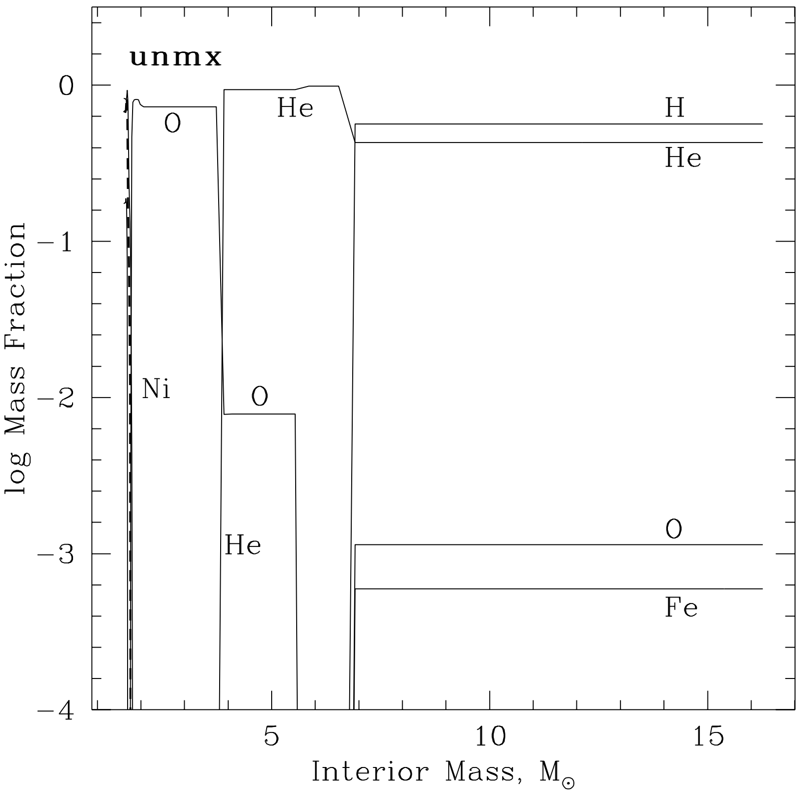


Fig. 2.— Composition as a function of interior mass, $M_r$, in the unmixed presupernova model unmx from Nomoto et al. (1988), mass cut is 1.6 M$_\odot$.



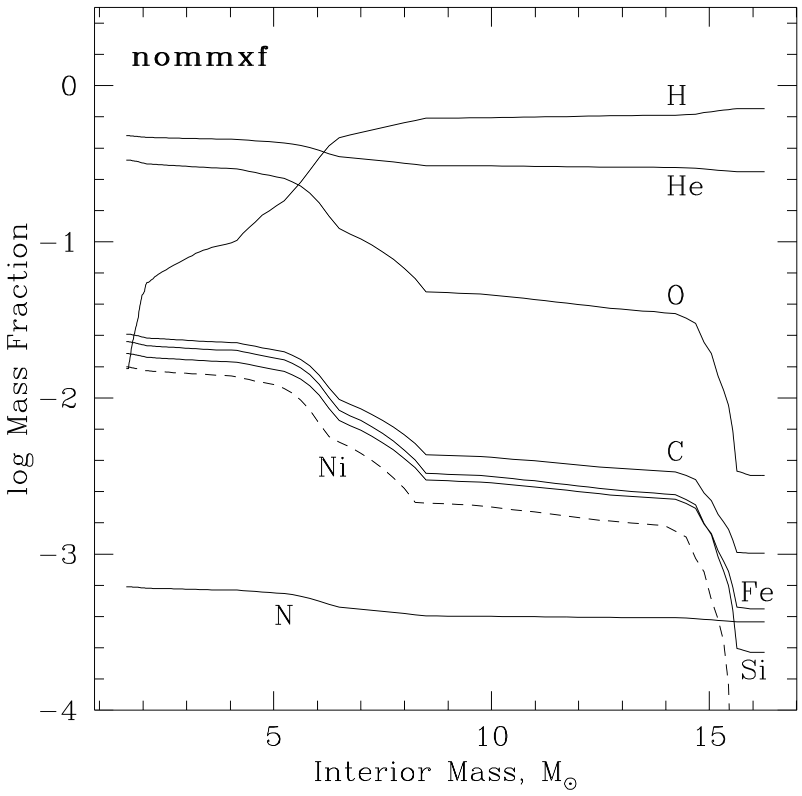


Fig. 3.— Composition as a function of interior mass, $M_r$, in the mixed model nommxf, mass cut is 1.6 M$_\odot$.

Another model was from Utrobin (1990). It is not an evolutionary model - it is constructed in the hydrostatic equilibrium with the chemical composition for the best fit of observed luminosity and photospheric parameters of SN 1987A. Since we get too much ultraviolet light in the realistic evolutionary of Nomoto & Hashimoto (1988), Saio, Nomoto & Kato (1988) nom, and since the chemical composition of heavy elements was not specified in Utrobin (1990) (only the mass distribution of $Z$ is given), we assumed an iron rich composition which allows us to get enhanced extinction in ultraviolet in iron lines.



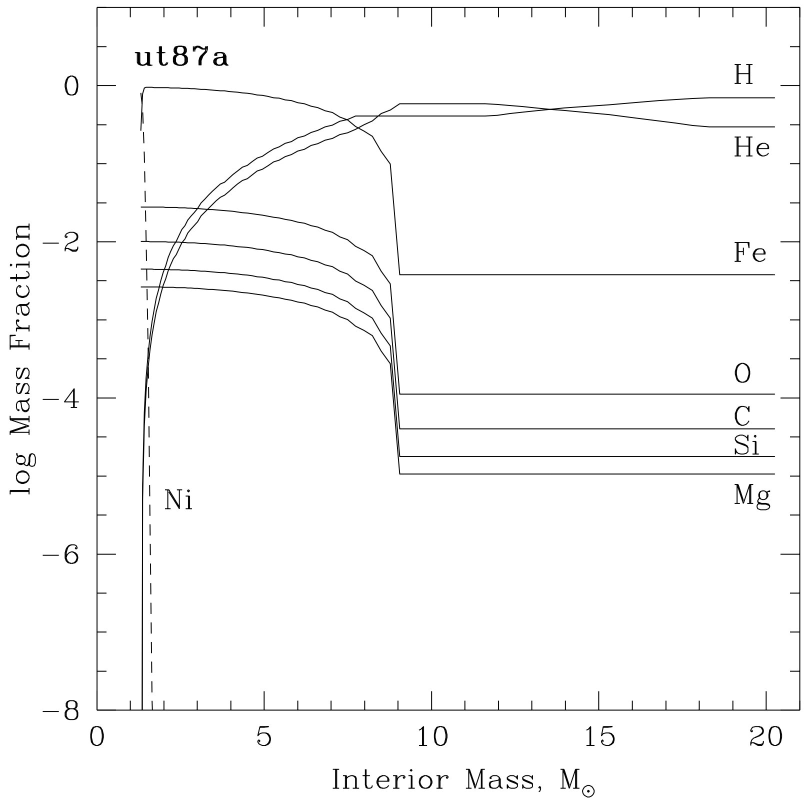


Fig. 4.— Composition as a function of interior mass, $M_r$, in the model ut87a, mass cut is 1.26 $M_\odot$.

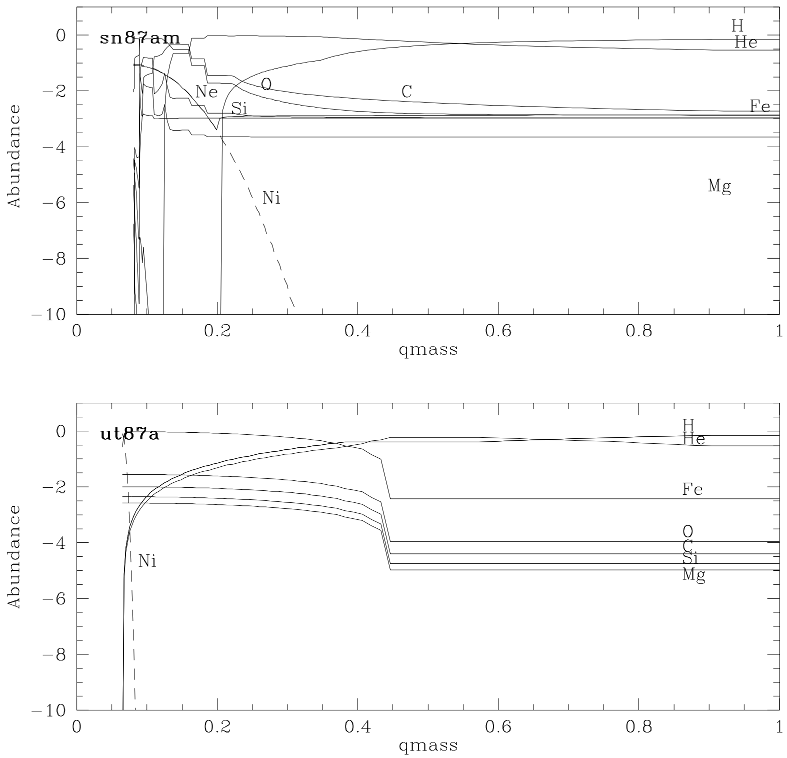


Fig. 5.— Comparison of chemical compositions for models ut87a and sn87am (Woosley, Weaver & Langer) as functions of interior mass normalized to the total mass, $q = M_r/M$ .



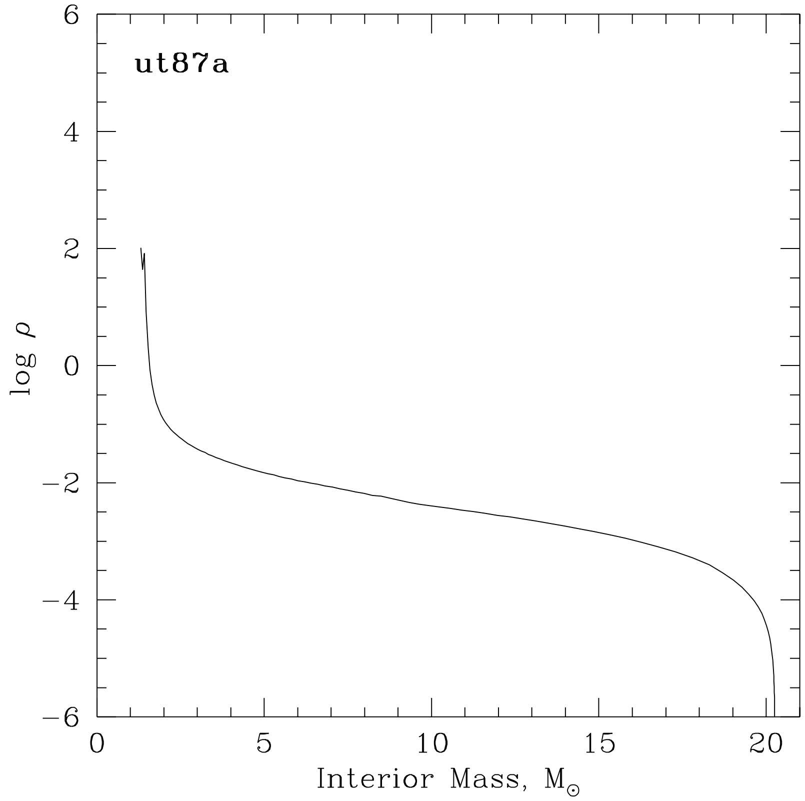


Fig. 6.— Density as a function of interior mass in the model ut87a, mass cut is 1.26 $M_{\odot}$.

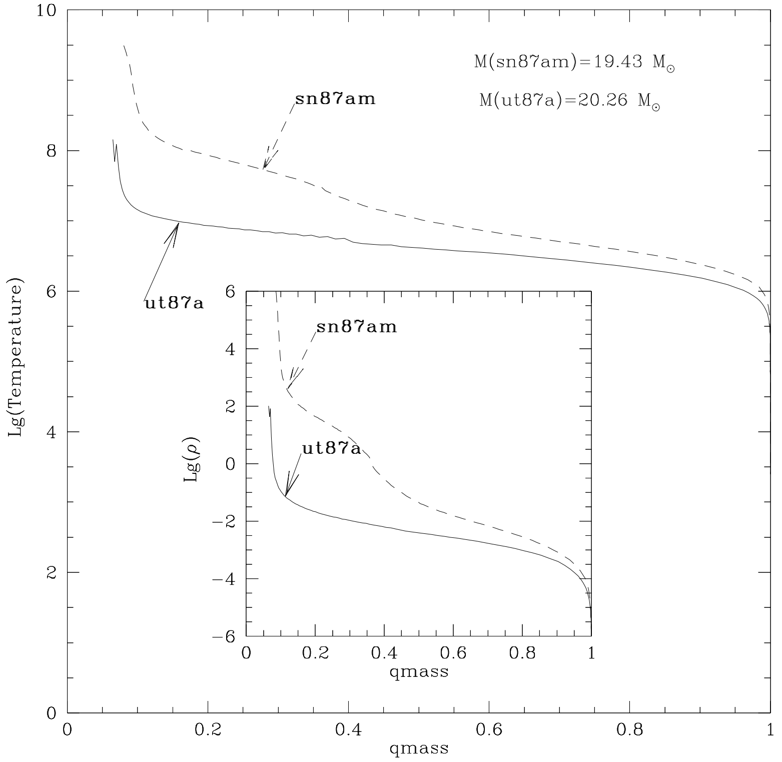


Fig. 7.— Comparison of density and temperature profiles for models ut87a and sn87am (Woosley, Weaver & Langer) as functions of interior mass normalized to the total mass, $q = M_r/M$ .



## 3. Coasting Phase Profiles

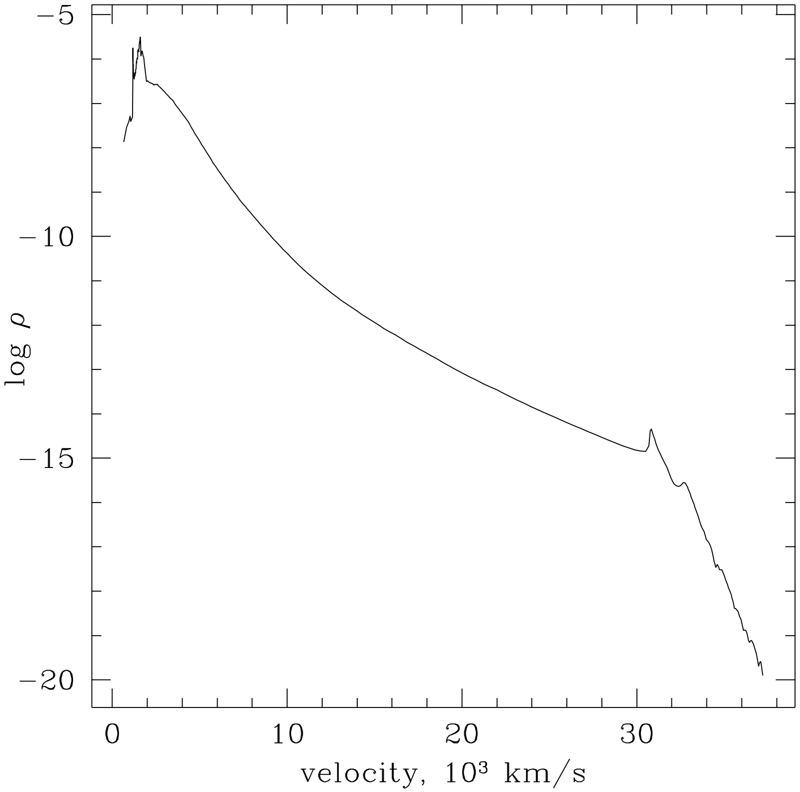


Fig. 8.— Density as a function of velocity in the mixed model nommxf at $t = 0.764$ days after explosion in the core (retarded observer time). The highest velocity reached is $37.2 \times 10^3$ km/s.



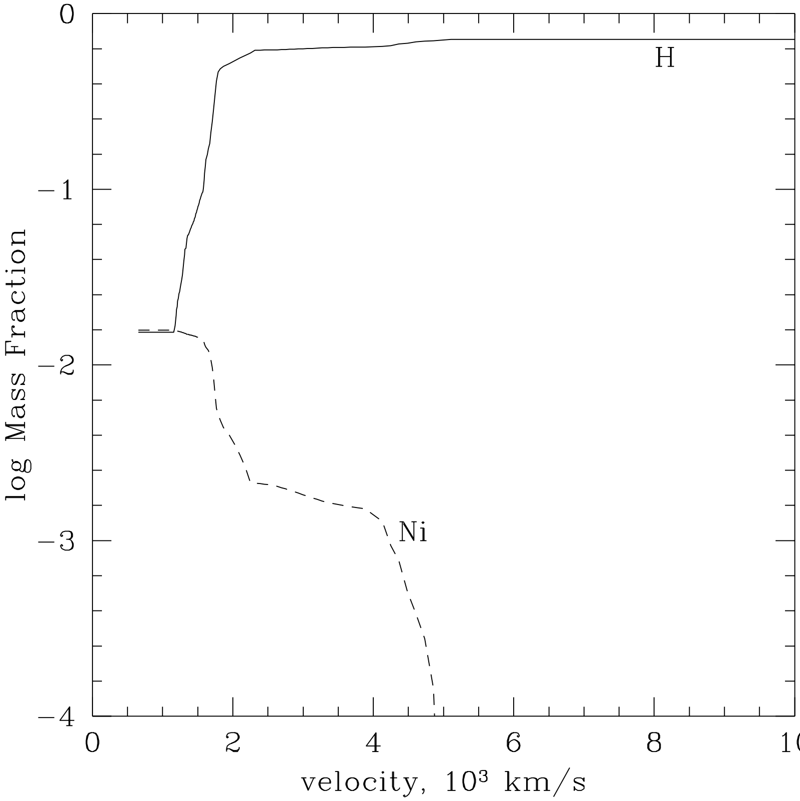


Fig. 9.— Hydrogen and "Nickel-56" distributions as a function of velocity in the layers of $u < 10^4$ km/s in the mixed model nommxf.

## 4. Shock Breakout



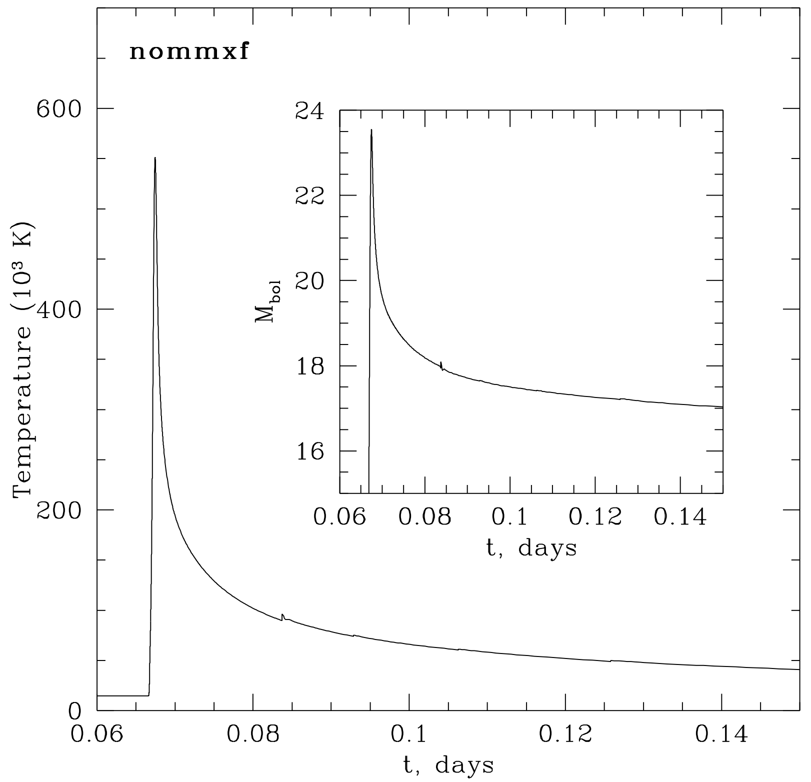


Fig. 10.— Very early bolometric light curve and effective temperature for nommxf model with realistic, scattering dominated opacity

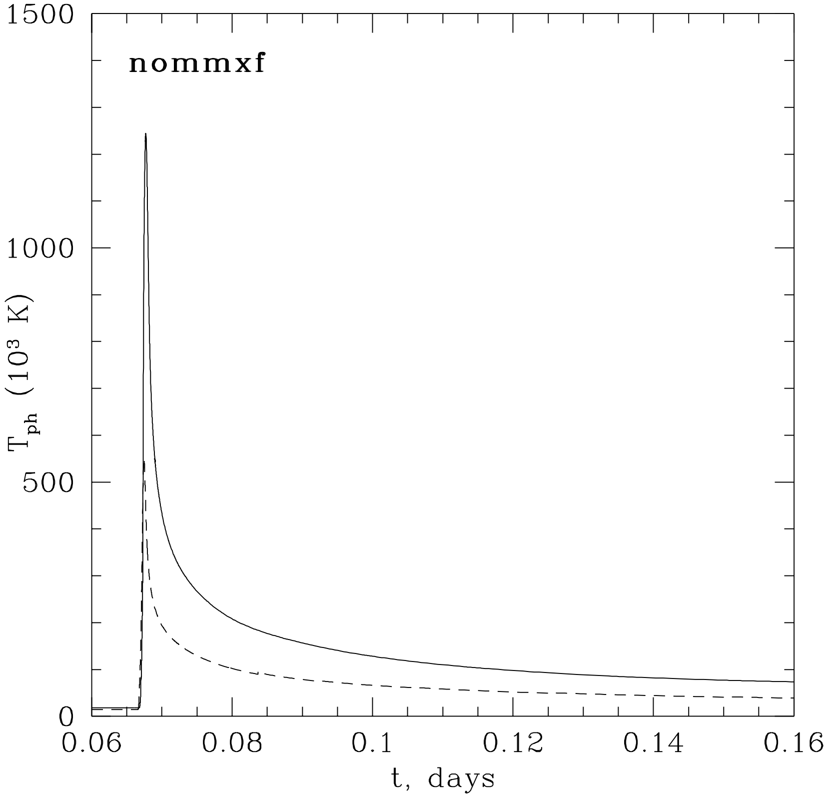


Fig. 11.— Very early photospheric temperature for nommxf model with realistic, scattering dominated opacity, solid line is the temperature of the best blackbody fit to the flux and the dashed one is the effective temperature defined by luminosity and the radius of last scattering



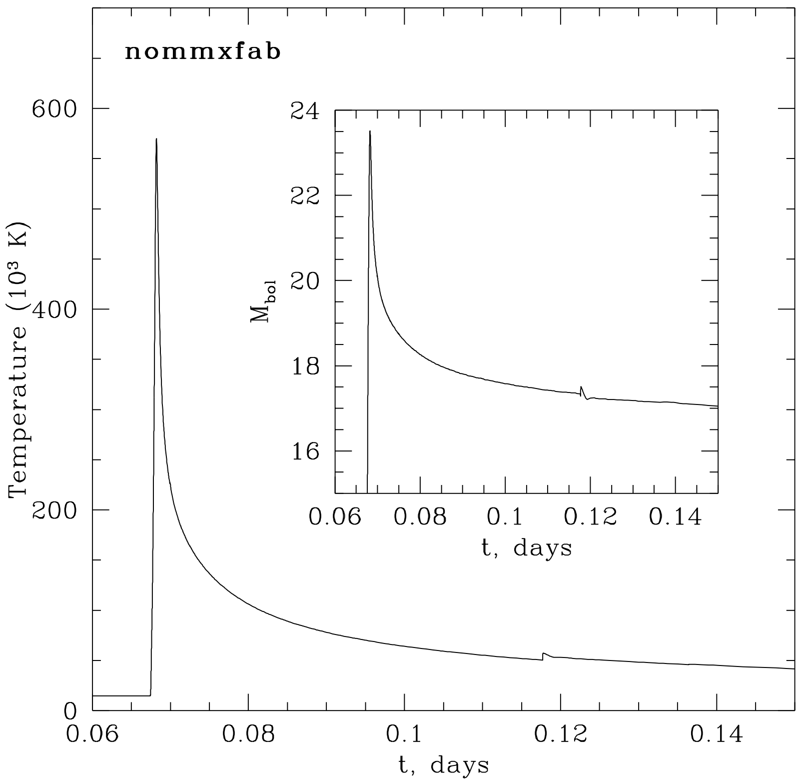


Fig. 12.— Very early bolometric light curve and effective temperature for nommxf model with forced absorption opacity

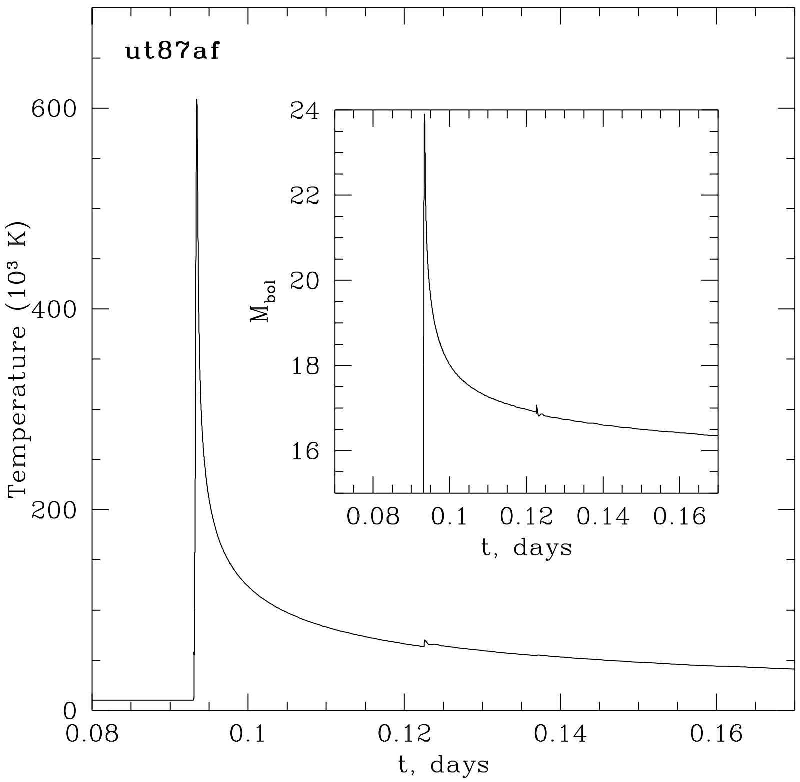


Fig. 13.— Very early bolometric light curve and effective temperature for ut87af model with realistic, scattering dominated opacity



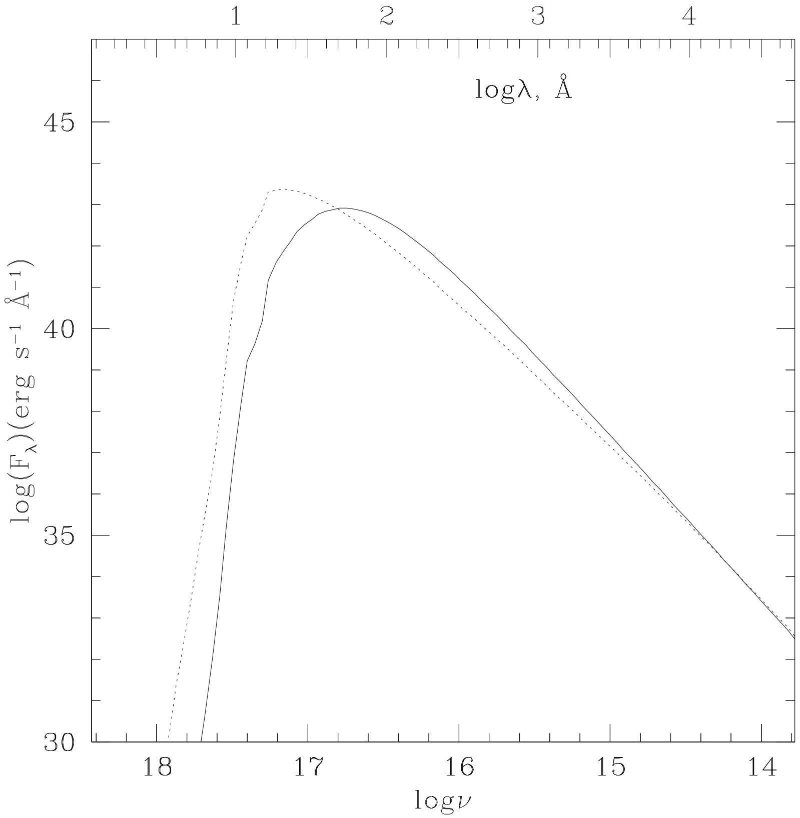


Fig. 14.— Spectral flux in the observer frame at first maximum light for $t$ = 0.0674 days (dashed) for model nommxf (scattering), $t$ = 0.0682 days (solid) for model nommxfab (absorption).

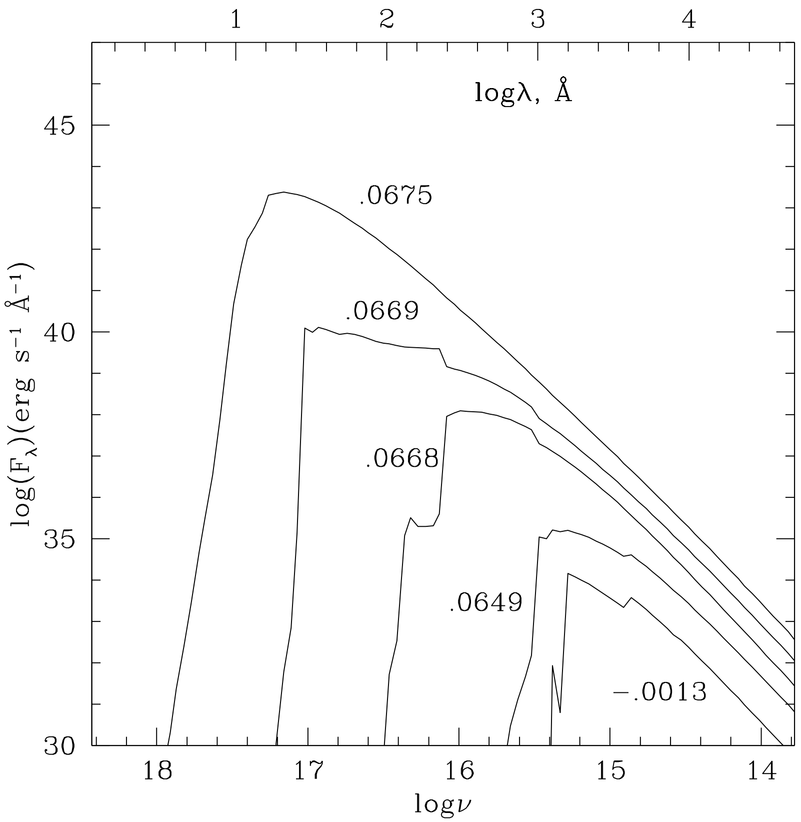


Fig. 15.— Spectral flux in the observer frame at at the shock breakout for the model nommxf. The curves are labeled by the retarded time in days.



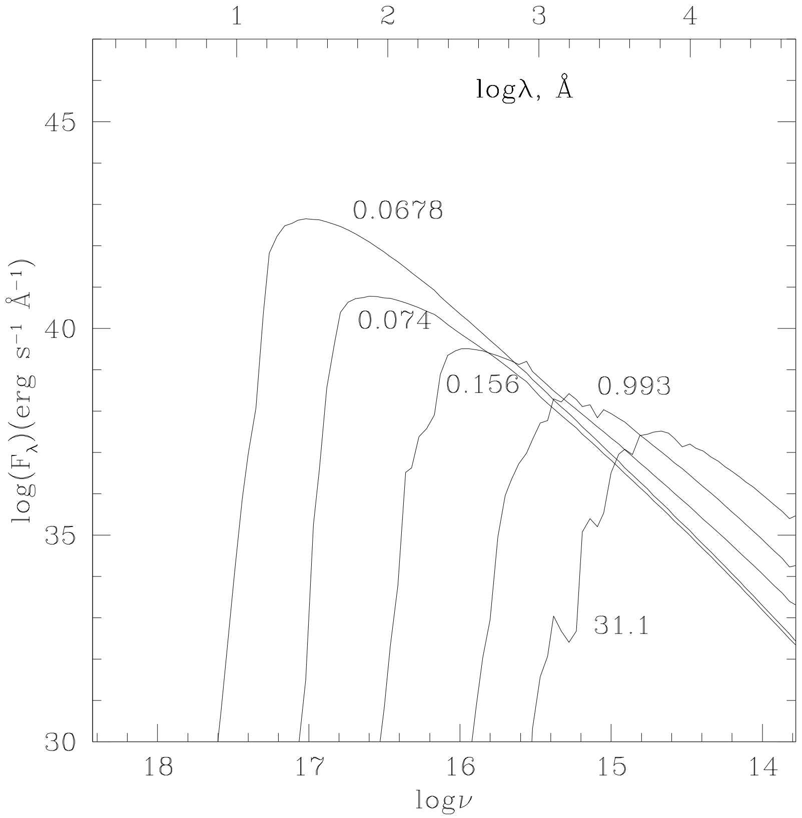


Fig. 16.— The same as in figure 15 but after the shock breakout.

**5. The first days**



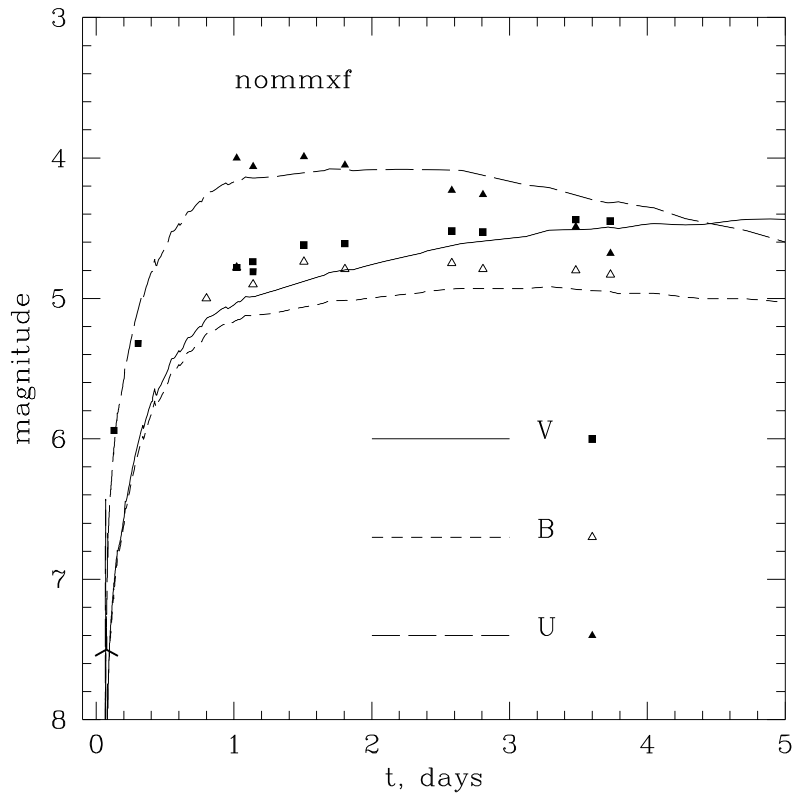


Fig. 17.— UBV fluxes in the observer frame reddened for $E_{BV} = 0.15$ and for distance modulus 18.5 for the model nommxf. Jones's limit is shown by inverted Y .

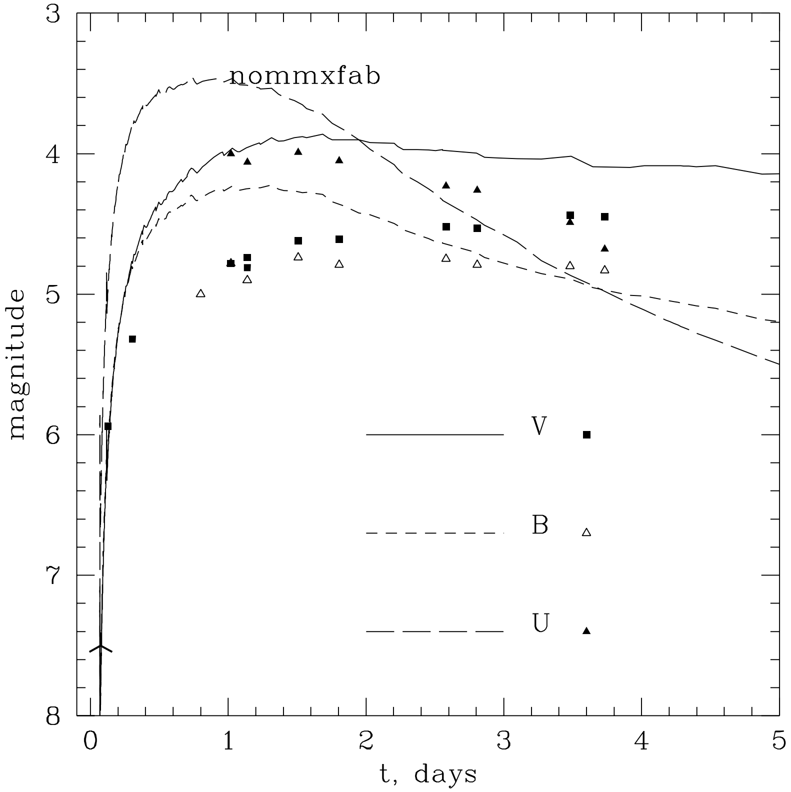


Fig. 18.— UBV fluxes in the observer frame reddened for $E_{BV} = 0.15$ and for distance modulus 18.5 for the model nommxfab (forced absorption) Jones's limit is shown by inverted Y .



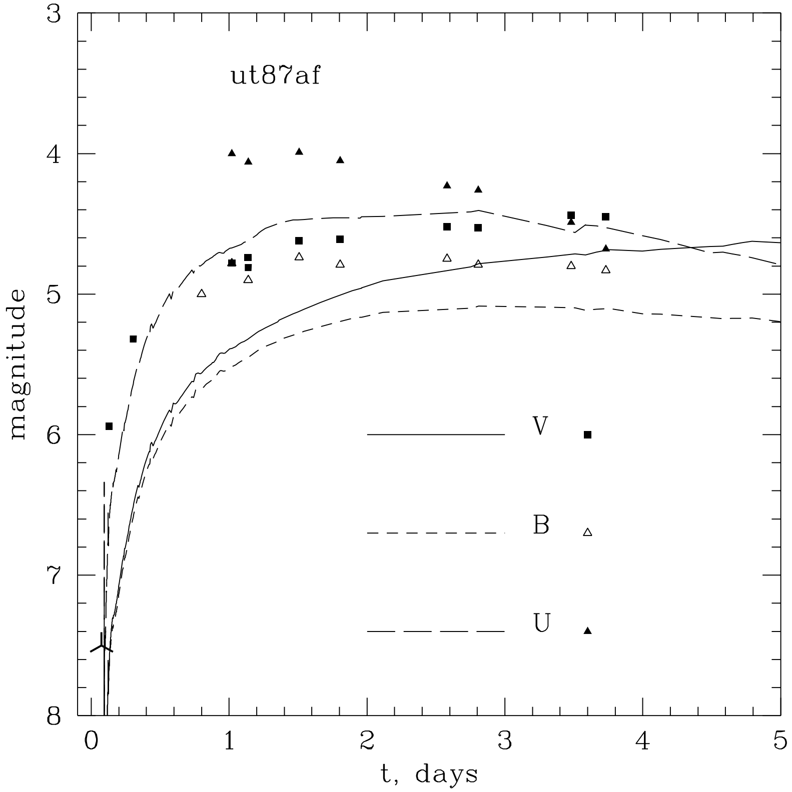


Fig. 19.— UBV fluxes in the observer frame reddened for $E_{BV} = 0.15$ and for distance modulus 18.5 for the model ut87af. Jones's limit is shown by inverted Y .

## 6. Bolometric Light Curves



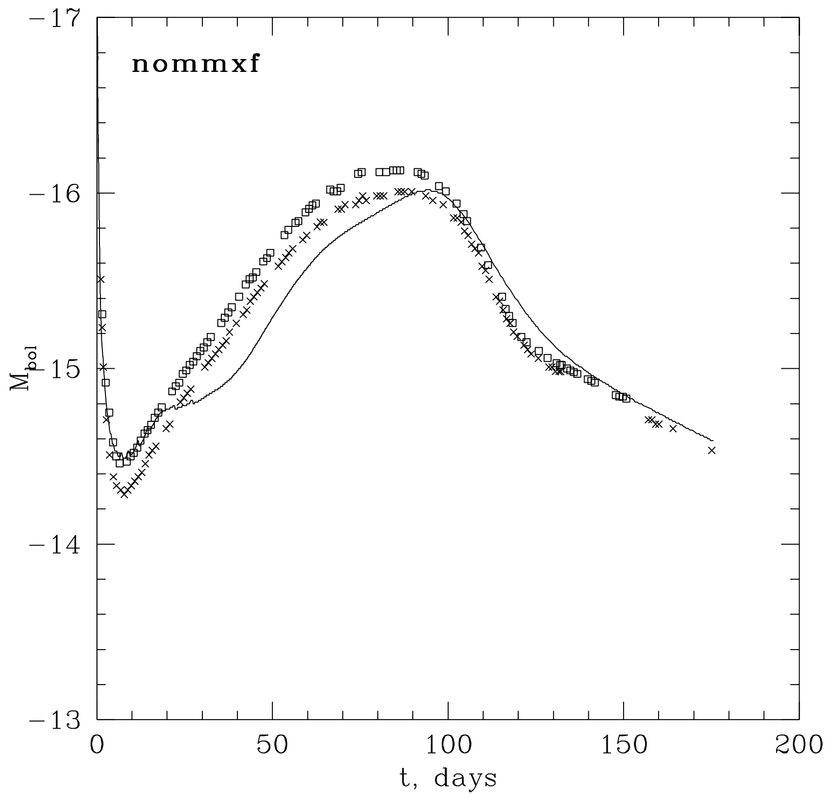


Fig. 20.— Bolometric magnitude for the model nommxf Nomoto et al. Squares are the data of Catchpole et al., crosses - Hamuy et al.

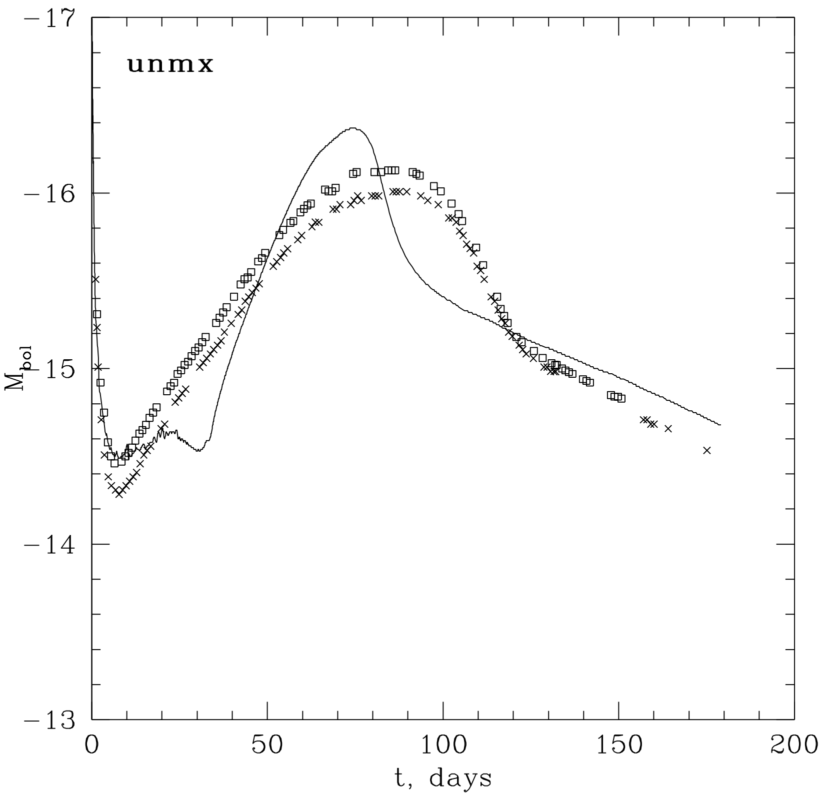


Fig. 21.— Bolometric magnitude for the unmixed model unmx of Nomoto et al. Squares are the data of Catchpole et al., crosses - Hamuy et al.



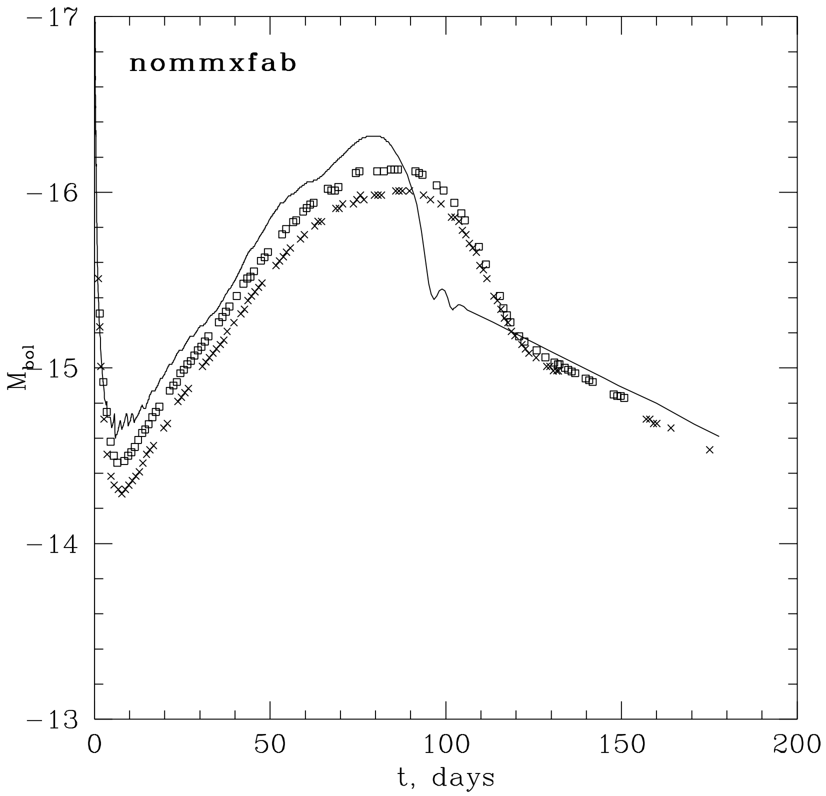


Fig. 22.— Bolometric magnitude for the model nommxfab (forced absorption instead of scattering). Squares are the data of Catchpole et al., crosses - Hamuy et al.

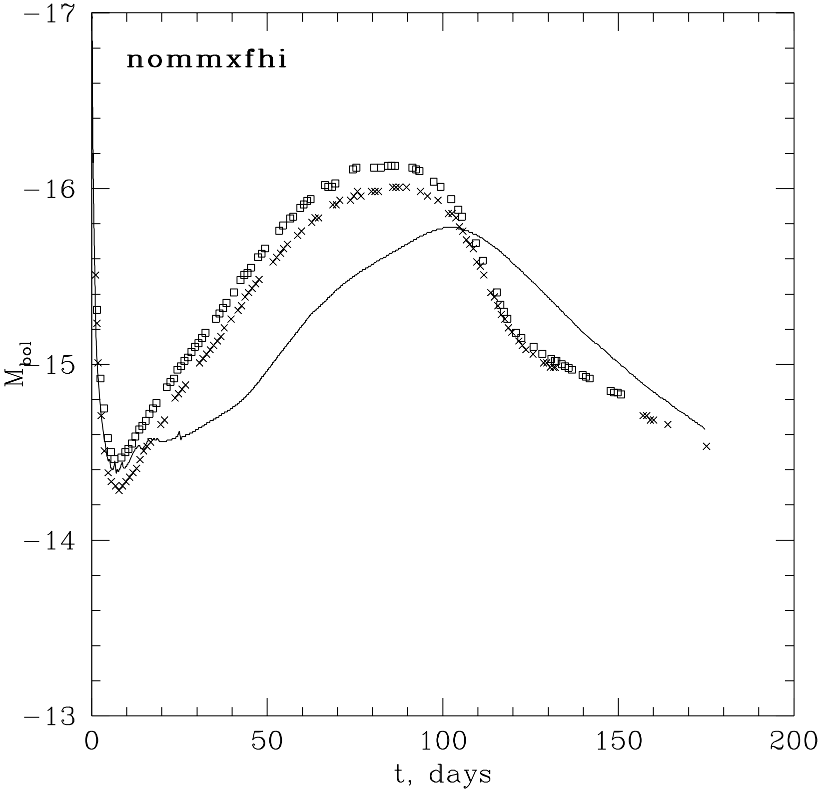


Fig. 23.— Bolometric magnitude for the model nommxfhi (scattering is treated correctly, but expansion opacity for high velocity gradient at $t_s = 1$ day is used everywhere). Squares are the data of Catchpole et al., crosses - Hamuy et al.



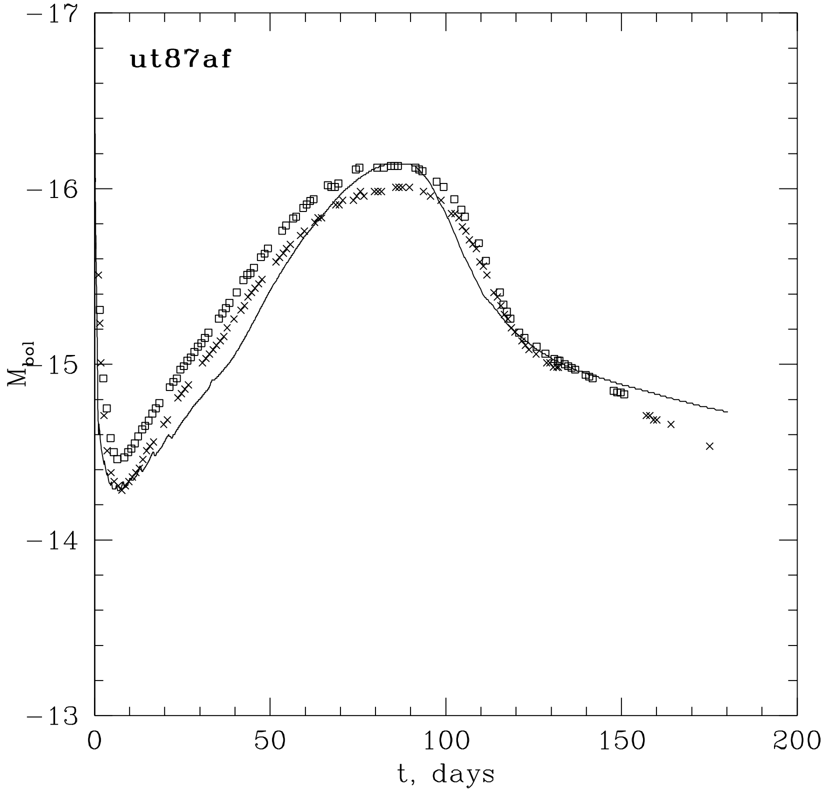


Fig. 24.— Bolometric magnitude for the model ut87af. Squares are the data of Catchpole et al., crosses - Hamuy et al.

## 7. UBV Photometry



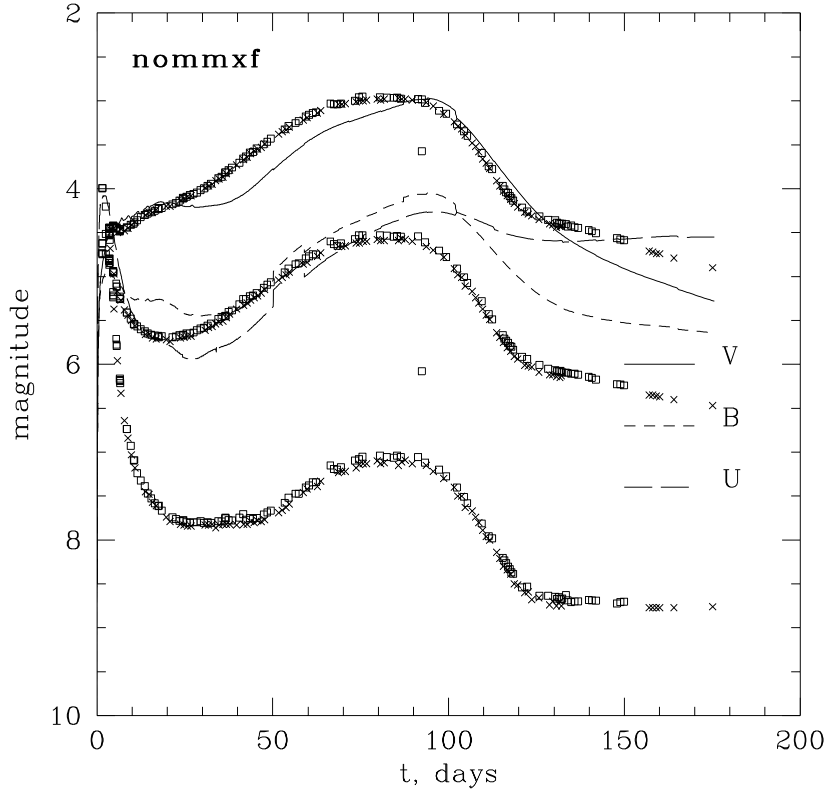


Fig. 25.— UBV magnitudes for the model nommxf of Nomoto et al. Squares are the data of Catchpole et al., crosses - Hamuy et al.

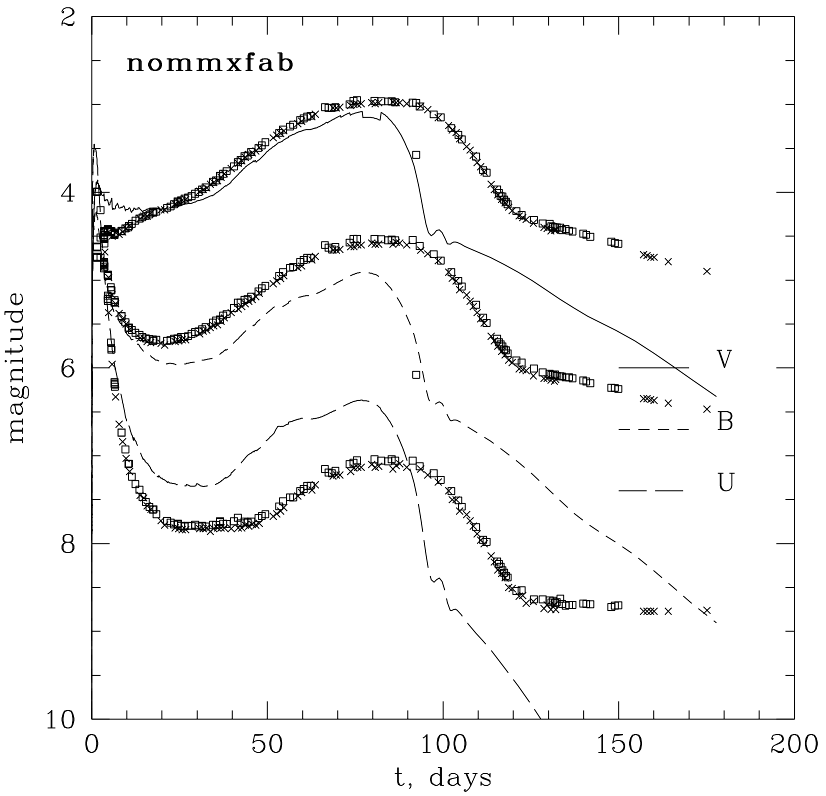


Fig. 26.— UBV magnitudes for the model nommxfab (forced absorption instead of scattering). Squares are the data of Catchpole et al., crosses - Hamuy et al.



## 8. Photospheric Fits

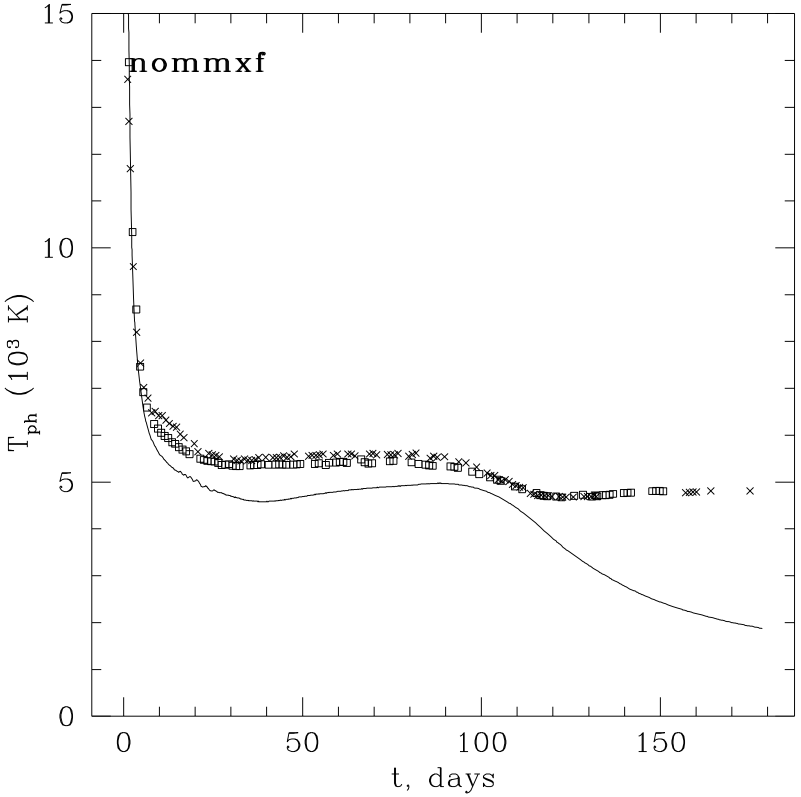


Fig. 27.— The solid line is the temperature $T_{\rm ph}$ of the best blackbody fit to the flux in the model nommxf of Nomoto et al. Squares are the data of Catchpole et al., crosses - Hamuy et al.



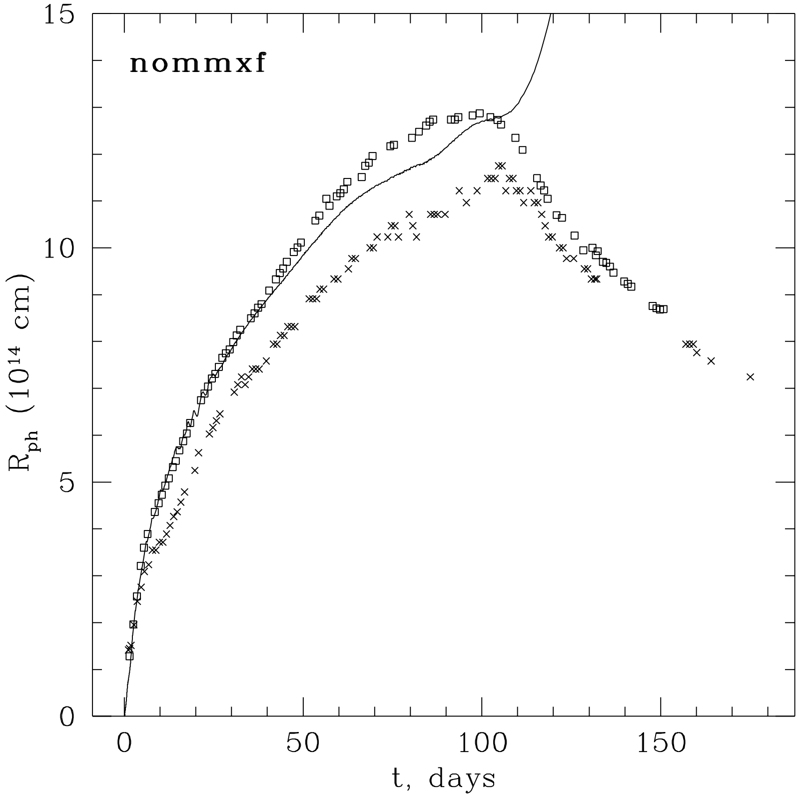


Fig. 28.— The photospheric radius $R_{\rm ph}^2$ defined by luminosity $L$ from the relation $L = 4\pi\sigma T_{\rm ph}^4 R_{\rm ph}^2$ for $T_{\rm ph}$ in the figure 27 Squares are the data of Catchpole et al., crosses - Hamuy et al.

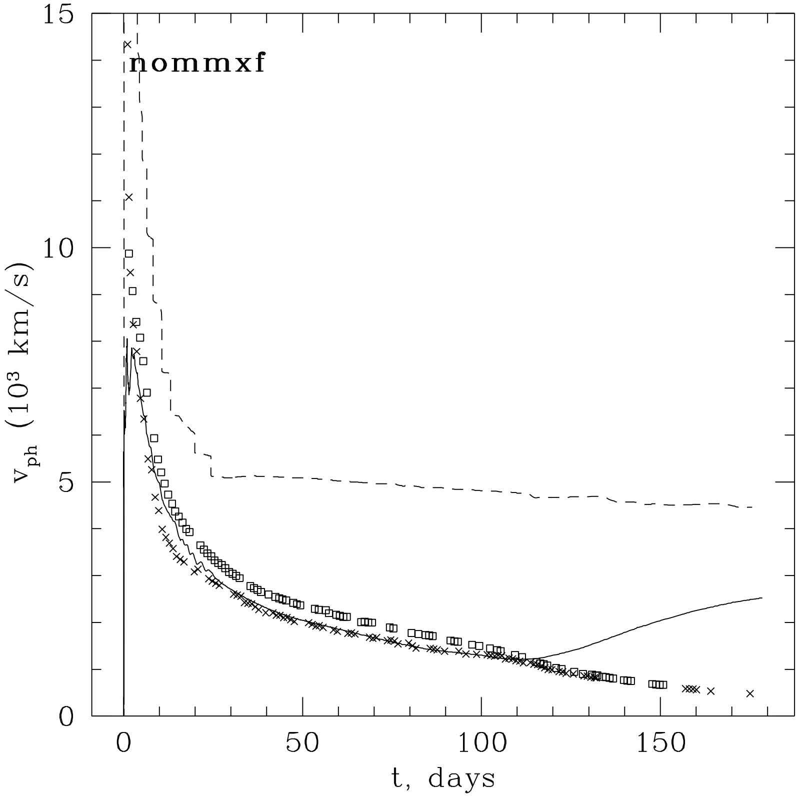


Fig. 29.— The solid line is the velocity at the radius $R^2_{\rm ph}$ in the figure 28. The dashed line is a crude estimate of velocity at the last scattering radius. Squares are the data of Catchpole et al., crosses - Hamuy et al. for their $R_{\rm ph}/t$



## 9. IUE Observations

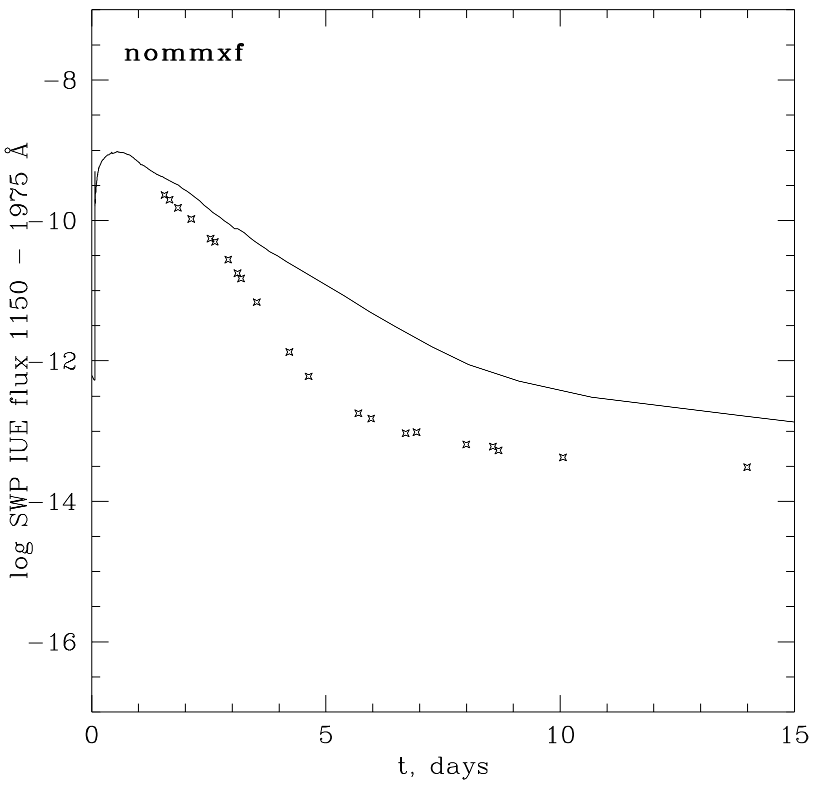


Fig. 30.— IUE SWP flux in the observer frame for distance modulus 18.5 for the model nommxf.



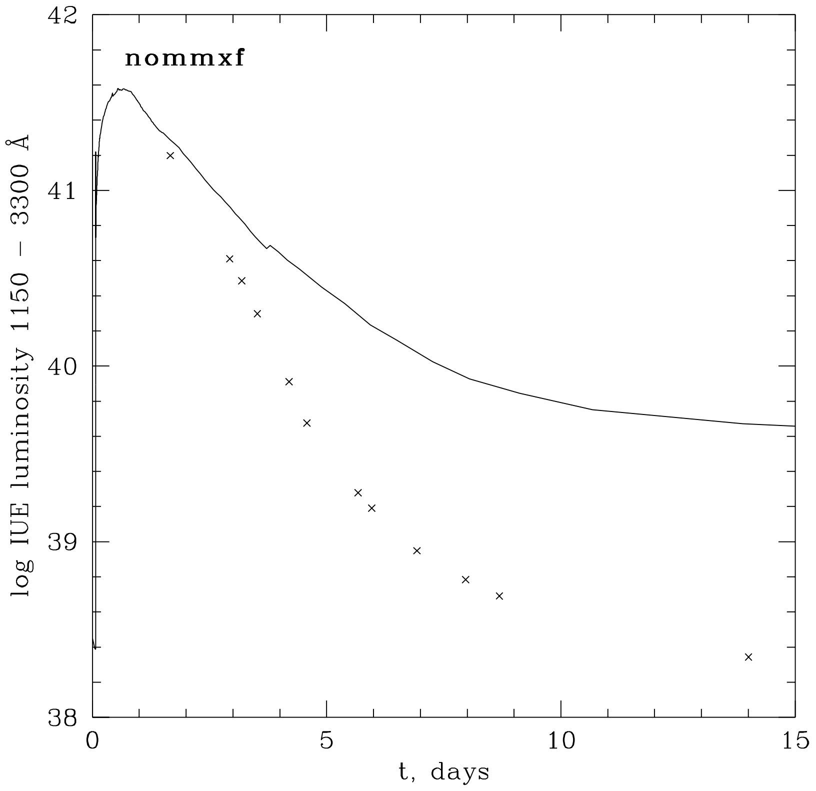


Fig. 31.— Total IUE luminosity flux in the observer frame for the model nommxf.

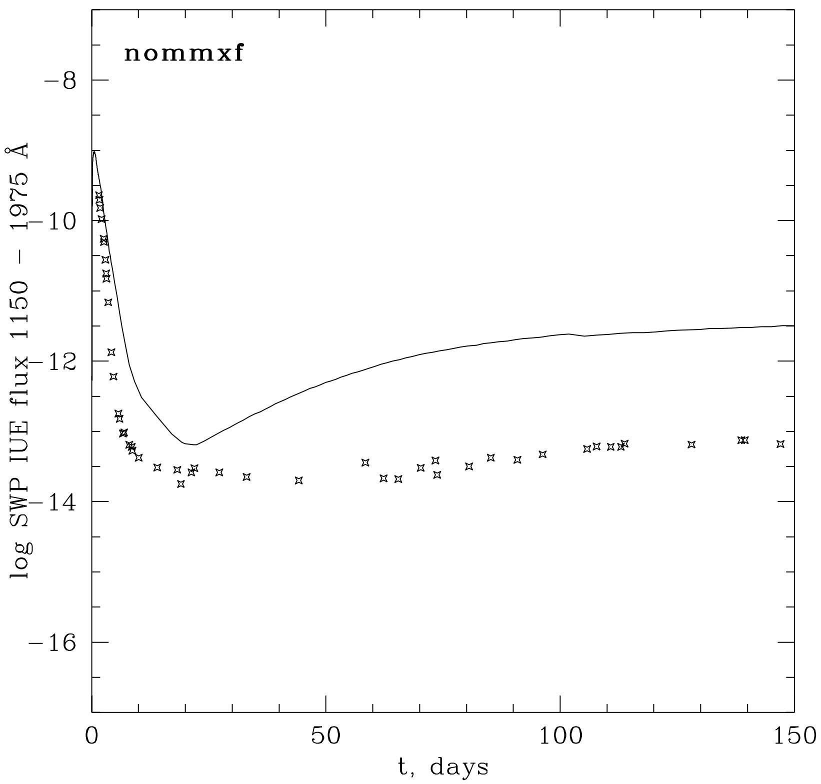


Fig. 32.— IUE SWP flux in the observer frame for distance modulus 18.5 for the model nommxf.



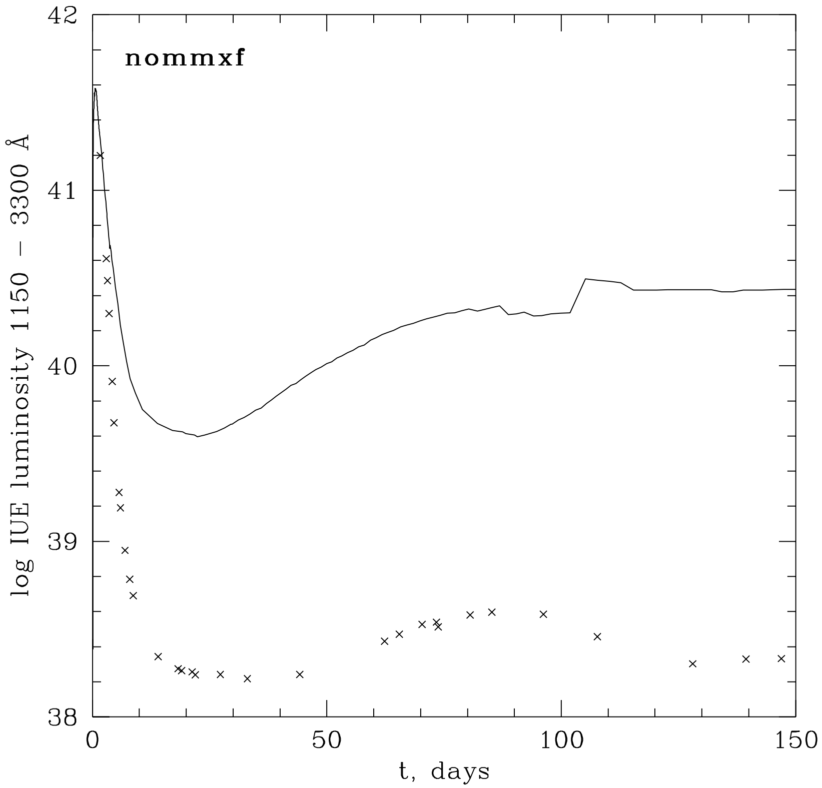


Fig. 33.— Total IUE luminosity flux in the observer frame for the model nommxf.

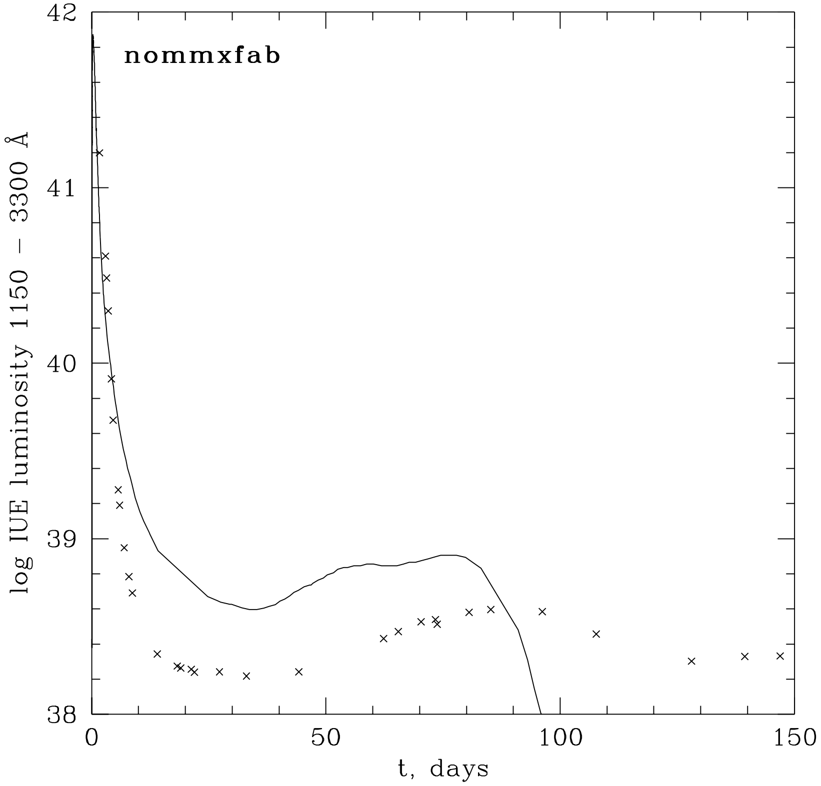


Fig. 34.— Total IUE luminosity flux in the observer frame for the model nommxfab (forced absorption instead of scattering).



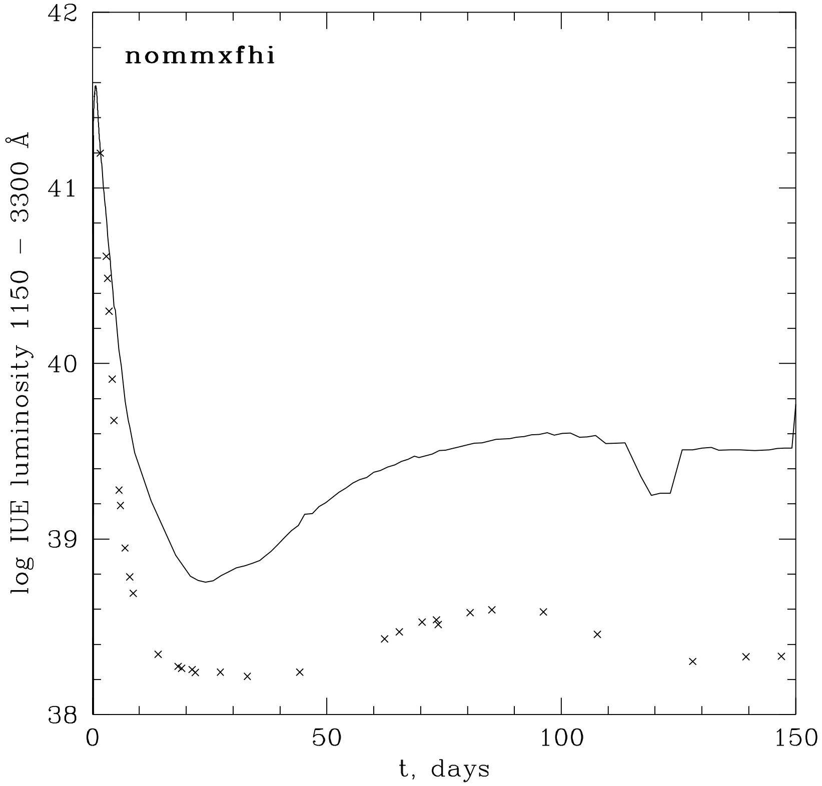


Fig. 35.— Total IUE luminosity flux in the observer frame for the model nommxfhi (scattering is treated correctly, but expansion opacity for high velocity gradient at $t_s = 1$ day is used everywhere).

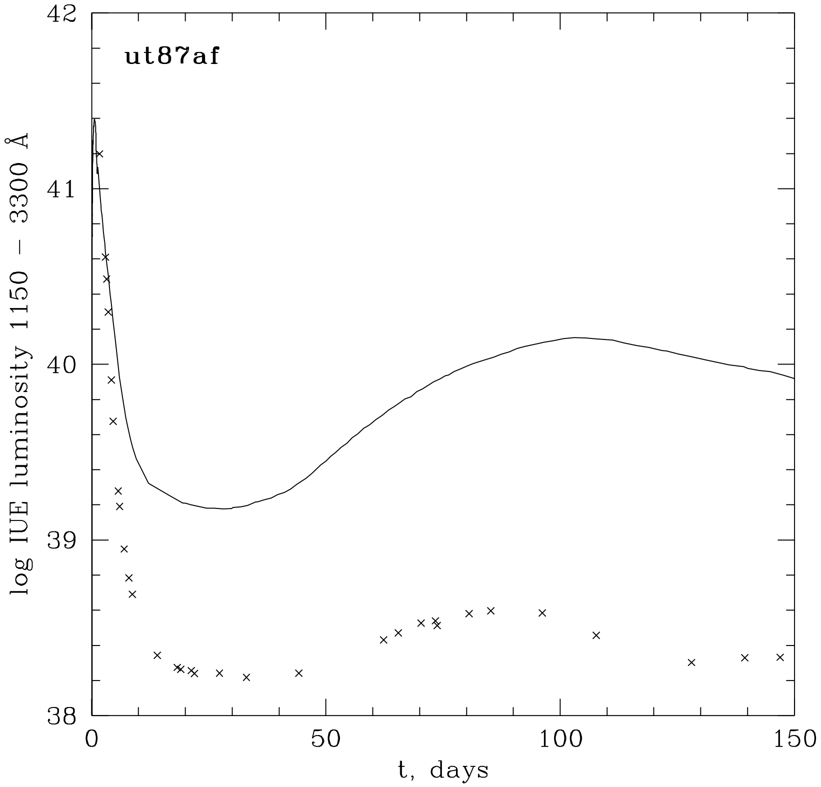


Fig. 36.— Total IUE luminosity flux in the observer frame for the model ut87af (scattering and expansion opacity treated correctly, but Fe is enhanced, see Figs 4,5 .



Table 1: Runs

| run | $M$ | $M_{\rm cut}$ | $R_0$ | $E_{\rm kin}$, foe | $N_{\rm zon}$ | forced $\chi_{\rm abs}$ | enhanced $\chi_{\rm exp}$ |
|---|---|---|---|---|---|---|---|
| nommxf | 16.27 | 1.6 | 48.5 | 1.3 | 300 | no | no |
| nommxfab | 16.27 | 1.6 | 48.5 | 1.3 | 300 | yes | no |
| nommxfhi | 16.27 | 1.6 | 48.5 | 1.3 | 300 | no | yes |
| nommixf | 16.27 | 1.6 | 48.5 | 1.3 | 200 | no | no |
| unmx | 16.27 | 1.6 | 48.5 | 1.3 | 200 | no | no |
| ut87af | 20.26 | 1.3 | 47. | 1.4 | 300 | no | no |